Molecular Dynamics Modeling of the Conductivity of Lithiated Nafion Containing Nonaqueous Solvents

Citation: Burlatsky, Sergei et al. "Molecular Dynamics Modeling of the Conductivity of Lithiated Nafion Containing Nonaqueous Solvents." Journal of The Electrochemical Society 163.10 (2016): A2232–A2239.

As Published: http://dx.doi.org/10.1149/2.0461610jes

Publisher: Electrochemical Society

Persistent URL: http://hdl.handle.net/1721.1/107626

Version: Final published version: final published article, as it appeared in a journal, conference proceedings, or other formally published context

Molecular Dynamics Modeling of the Conductivity of Lithiated Nafion Containing Nonaqueous Solvents

Sergei Burlatsky,[a,b,*] Robert M. Darling,[a,b,*,z] Dmitri Novikov,[a,b] Vadim V. Atrazhev,[c,d] Vadim I. Sultanov,[d] Tatiana Y. Astakhova,[c,d] Liang Su,[a,e] and Fikile Brushett[a,e,*]

[a]*Joint Center for Energy Storage Research*
[b]*United Technologies Research Center, East Hartford, Connecticut 06108, USA*
[c]*Russian Academy of Science, Institute of Biochemical Physics, Moscow 119334, Russia*
[d]*Science for Technology LLC, Moscow 119334, Russia*
[e]*Department of Chemical Engineering, Massachusetts Institute of Technology, Cambridge, Massachusetts 02139, USA*

We use molecular dynamics to predict the ionic conductivities of lithiated Nafion perfluorinated ionomeric membranes swelled in dimethyl sulfoxide (DMSO) and acetonitrile (ACN). The experimental conductivity of lithiated Nafion swollen with DMSO is two orders of magnitude higher than with ACN. Conversely, the mobility of Li^+ ions in a solution of $LiPF_6$ in ACN is approximately six times higher than in DMSO. In this work, we demonstrate that the ionic conductivity of Nafion is substantially governed by the concentration of free Li^+ ions, i.e. by the degree of dissociation of the Li^+ and SO_3^- pairs, and that the inherent mobility of Li^+ in different solvents is of secondary importance.

Manuscript submitted October 7, 2015; revised manuscript received July 26, 2016. Published August 11, 2016.

Nafion is a cation-exchange membrane that has been extensively studied and used in aqueous electrochemical systems. In this work, we seek to understand the applicability of Nafion to flow batteries that use nonaqueous solvents and lithium salts. A flow battery is an electrochemical device that stores and releases energy by oxidizing and reducing redox molecules that remain dissolved in electrolytes. The active molecules are stored in external vessels and pumped to reactors to charge or discharge the battery. This arrangement provides a separation of energy and power that is absent from conventional enclosed batteries like lead acid. The all-vanadium redox flow battery, for example, is an aqueous system that relies on the V^{2+}/V^{3+} and VO^{2+}/VO_2^+ couples at the negative and positive electrodes and H^+ as the primary charge carrier. Nonaqueous electrolytes are being considered for redox flow batteries to enable electrochemical couples with potential differences substantially exceeding the aqueous stability limit of 1.23 V, and, consequently, increase energy density. Two key considerations in reactor design are power density and Coulombic efficiency. The membrane must possess high ionic conductivity, low electronic conductivity, and low permeability of active species (the various vanadium ions in the aqueous example mentioned above) to simultaneously achieve high area-specific power density and high Coulombic efficiency. In this work, Li^+ is the primary charge carrier, and the unspecified active species are assumed to be absent from the membrane. Future work could examine the behavior of active molecules in lithiated membranes containing different solvents, with a specific focus on the charge on the active molecule.

Many experimental[1–9] and numerical[10–21] works discussing ion diffusion and conductivity in Nafion swollen with water have been published during the past two decades. The dependence of conductivity on water content and temperature is well understood. Furthermore, a number of theoretical[22,23] and experimental works consider Nafion swollen with methanol or water/methanol mixtures in the context of direct methanol fuel cells.[24,25] It has been demonstrated that the diffusion coefficients of water, methanol, and hydronium decrease with increasing methanol concentration. There have been far fewer studies on Nafion containing solvents other than water and methanol. A notable exception is the experimental work of Doyle et al. that evaluates the conductivity of lithiated Nafion (N117) in contact with a variety of nonaqueous solvents in the context of lithium-ion batteries.[26]

Two exemplary solvents, dimethyl sulfoxide (DMSO) and acetonitrile (ACN), were simulated in this work. The measured conductivity of lithiated Nafion (Li-N117) is approximately two orders of magnitude higher in DMSO than in ACN according to Doyle et al.,[26] however a recent paper reported a much higher conductivity for lithiated Nafion (N1035) soaked in ACN.[27] This discrepancy motivated us to reproduce these conductivity measurements. The mobility of Li^+ ions in an electrolyte solution consisting of $LiPF_6$ in ACN is approximately six times higher than in a solution of $LiPF_6$ in DMSO.[28,29] Therefore, if the measurements of Doyle et al. are correct, the conductivity of lithium in an electrolyte is not strongly correlated with the conductivity of lithiated Nafion containing the same solvent. The two solvents DMSO and ACN are potentially suitable for battery electrolytes, and understanding what limits the conductivity of Nafion in their presence should provide more general insights about solvent selection and performance limits.

Molecular dynamics simulations of lithium solvation in DMSO/ACN mixtures of varying mole fractions were reported by Semino et al.[30] Available molecular dynamics force fields for liquid phases of DMSO and ACN were analyzed in the referenced work, and an optimal set of parameters was determined. These parameters satisfactorily describe both structural properties of DMSO/ACN mixtures and experimental coordination numbers of Li^+ in pure DMSO and ACN. We used these parameters in our simulations of lithiated Nafion. The numerical simulations presented in Ref. 30 are in satisfactory agreement with experimentally determined ionic conductivities of $LiPF_6$ in DMSO/ACN mixtures.[28] Simulation and experiment both show that Li^+ ions are preferentially solvated by DMSO in DMSO/ACN mixtures. Hence, the solvation energy of a Li^+ ion by DMSO is much higher than by ACN. On the other hand, the higher solvation energy of Li^+ ions by DMSO leads to lower mobility in DMSO than in ACN.

Previous experimental investigations have examined the ionic conductivities of polymers containing SO_3^- groups and non-aqueous solvents.[26,31–33] Conductivity was generally observed to increase with solubility parameter, dielectric constant, and amount of solvent, and decrease with the equivalent weight (EW) of the ionomer. However, many exceptions were observed and large variations in performance were found from the many different solvents, necessitating an understanding of how individual solvent properties contribute to overall performance. An exhaustive summary of experimental ionic conductivities of the lithium form of Nafion swollen in different solvents can be found in Reference 26. For clarity, we plot the experimental

*Electrochemical Society Member.
[z]E-mail: darlinrm@utrc.utc.com

conductivities from Reference 26 as a function of equilibrium solvent uptake for different solvents in Figure 1 of the supplementary material. This plot shows that Nafion conductivities in solvents with similar uptakes can differ by more than an order of magnitude. For example: in Nafion dibutylamine (DBA) demonstrates a solvent uptake of 51% and an ionic conductivity of 0.14 mS/cm, while dimethylacetamide (DMA) demonstrates an uptake of 45% and ionic conductivity of 3 mS/cm.

The objectives of this work are to analyze the diffusivity and conductivity of lithiated Nafion swollen with two exemplary nonaqueous solvents. Having reliable predictive means for designing battery systems can provide molecular level insight into laboratory experiments as well as provide direct screening capabilities to determine which effects and solvents are contributing significantly to performance. In this paper, we compare experimental results with molecular dynamics calculations of the structure, diffusivity, and conductivity of lithiated Nafion swollen with either DMSO or ACN.

Experimental

The conductivities of Li-N117 in 0.1 mol/L $LiPF_6$ in acetonitrile and dimethylsulfoxide were measured to compare to the simulations and to address the discrepancy in the Nafion + ACN conductivity data in the literature. Anhydrous ACN and DMSO were purchased from Sigma-Aldrich. Lithium hexafluorophosphate ($LiPF_6$) was purchased from BASF. The electrolytes were dried over 3 Å molecular sieves (Sigma-Aldrich) for at least 24 hours before use. Pristine Nafion 117 membrane (N117, in the proton form) was purchased from Ion Power. The lithiation of the pristine N117 was performed in the following sequence: the membrane was first placed in a boiling bath of 3% hydrogen peroxide (Fisher Chemical) for 1 hour, followed by placing the membrane in boiling 0.25 M sulfuric acid (Sigma-Aldrich) for 1 h, next the membrane was cleaned in boiling deionized water for 30 min three times, after which it was placed in boiling 0.25 M lithium hydroxide (Sigma-Aldrich) for 1 h, followed by cleaning in boiling DI water for 30 min three times, and finally the Li-N117 was dried at 120°C under vacuum for 6 days and transferred into the glove box.

The dried Li-N117 was soaked in solvent for 3 days and then in 0.1 M $LiPF_6$ plus solvent for another 3 days prior to the conductivity measurements. The thickness (t) of each membrane was measured using an electronic caliper (Mitutoyo, with an accuracy of 10 μm). The through-plane ionic conductivity of the Li-N117 soaked in different electrolytes was measured in an H-cell. The electrodes were graphite rods with an electrode-to-electrode distance of 6 cm. Cell resistances were measured using current interrupt at 0.1 mA for 0.05 s on a Bio-Logic VMP 3 potentiostat. The membrane conductivity (σ, mS/cm) was calculated as: $\sigma = \frac{1000 \cdot t}{(R_2 - R_1) \cdot A}$, where R_2 and R_1 are measured cell resistances (Ω) with and without a membrane, respectively, t is the thickness of the membrane after soaking in the electrolyte (0.1 M $LiPF_6$ + solvent), and A is the area of membrane (2 cm^2) perpendicular to the thickness. All measurements were replicated on three independent membrane samples at room temperature (~25°C).

Molecular Dynamics Model

Force field.—Force fields used in this work were obtained from three sources sharing the same functional form for interactions. In this functional form, the total potential energy of the system is presented as a sum of non-bonded and bonded parts:

$$U = U_{non-bonded} + U_{bonded}$$

The non-bonded part is a sum of electrostatic (Coulombic) and van der Waals energies:

$$U_{non-bonded} = U_{coul} + U_{vdw}$$

The electrostatic energy is expressed through Coulomb's law with partial charges q_i assigned to the individual atoms:

$$U_{coul} = \sum_{i \neq j} q_i q_j / r_{ij}$$

where the subscripts i and j denote the atom pairs, and r_{ij} is the distance between atoms i and j. The van der Waals energy is expressed by a Lennard-Jones potential

$$U_{vdw} = \sum_{i \neq j} 4\varepsilon_{ij}[(\sigma_{ij}/r_{ij})^{12} - (\sigma_{ij}/r_{ij})^{6}]$$

where pairwise constants ε_{ij} and σ_{ij} are calculated from per-atom constants ε_i and σ_i with the Lorentz-Berthelot combining rules:

$$\varepsilon_{ij} = \sqrt{\varepsilon_i \varepsilon_j}, \quad \sigma_{ij} = (\sigma_i + \sigma_j)/2$$

The bonded part of the potential energy is comprised of the following three terms:

1. Energy of chemical bonds stretching in harmonic form $U_{bonds} = \sum_b k_b (r_b - r_b^0)^2$, where b is the bond index, k_b is the force constant and r_b^0 is the equilibrium bond length.
2. Energy of bending angles formed by two chemical bonds sharing one of the participant atoms in harmonic form $U_{angles} = \sum_a k_a (\theta_a - \theta_a^0)^2$, where a is the angle index, k_a is the force constant and θ_a^0 is the equilibrium angle measure.
3. Energy of twisting dihedral angles formed by planes in which two angles sharing a common chemical bond lie in the form of a truncated Fourier series $U_{dihedrals} = \sum_d \sum_{n=1}^{3} k_d^{(n)}[1 + \cos(n\phi_d)]$, where d is the dihedral angle index and $k_d^{(n)}$ is the force constant.

The TEAM force field of Li et al. was used for the PFSA ionomer (Nafion),[39] because previous simulation results by Sun et al.[19] using the TEAM force field are in good agreement with experimental results. Force field parameters for the Li^+ cation, dimethyl sulfoxide and acetonitrile were taken from the work of Semino et al.[30] These authors searched the literature for combinations of force fields for each of the species that reproduced experimental coordination numbers of Li^+ in pure DMSO and ACN. The resulting combination comprised the Strader-Feller (FS) potential for DMSO[40] and the "A model" for ACN, developed by Nikitin and Lyubartsev,[41] along with the Li^+ parameters proposed by Dang.[42] The LAMMPS software package[43] was used for molecular dynamic simulations with Nose-Hoover style thermostat and barostat.

Simulation details.—To validate the force-field for DMSO, the self-diffusion coefficient was simulated. A system comprised of 500 DMSO molecules with periodic boundary conditions was simulated following Reference 30. The purpose of performing molecular dynamics in this small system was to quickly explore possible methods to accelerate the calculations without compromising physical fidelity.

The calculations of charge effects used the Particle-Particle Particle-Mesh technique (PPPM)[44] with a cutoff of 12 Å and force accuracy of 10^{-5}. In LAMMPS PPPM, force accuracy refers to mean square error in per-atom long range coulombic forces relative to the force that two unit point charges exert on each other at a distance of 1 Å. The accuracy of these parameters for the diffusion calculations was verified from a simulation of 500 DMSO molecules initially at a very low density (0.189 g/cm^3). NPT dynamics were conducted and the system equilibrated for 2 ns, where a density of 1.10 g/cm^3 was found which is equal to the experimental density. Next, the diffusion coefficient was calculated for pure DMSO. The result was 6.29 × 10^{-6} cm^2/s, which is close to the reported diffusion coefficient of 5 × 10^{-6} cm^2/s.[30] The simulation time step was varied to determine the maximum step size possible without significantly reducing the reliability of the diffusion calculations. The first set of calculations was

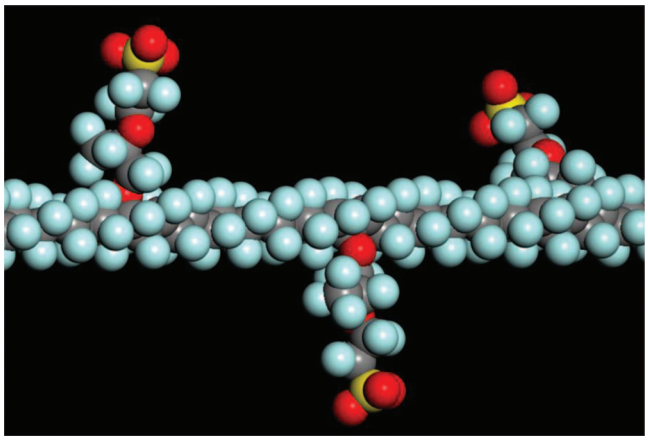

Figure 1. Portion of a PFSA chain with three side chains before thermalization. Carbon atoms are gray, fluorine atoms are blue, oxygen atoms are red, and sulfur atoms are yellow.

completed with a time step of 0.1 fs; however, using a time step of 0.8 fs resulted in a diffusion coefficient for DMSO of 6.33×10^{-6} cm^2/s. As the difference is minimal (<1%), an integration time step of 0.8 fs was used in the remainder of the simulations.

The PFSA chains were constructed on the basis of ideal PTFE chains with helical symmetry and a period of 13 monomers. One PFSA chain consists of 150 CF_2 backbone monomers and 10 side chains, which yields the correct equivalent weight (1100 g/eq). The initial structure of one PFSA chain before thermalization is shown in Figure 1. The initial configuration for thermalization consisted of 27 PFSA chains, 270 Li^+ ions (one per SO_3^- group), and either 5170 dimethyl sulfoxide molecules or 1376 acetonitrile molecules. A cube of size ($612 \times 612 \times 612$ Å^3) with periodic boundary conditions was chosen as the initial simulation box. Solvent molecules were randomly distributed in the simulation box. PFSA chains were oriented along the x or y or z axis and the positions of the chain centers were randomly distributed. The initial configuration before thermalization is shown in Figure 2.

The number of solvent molecules was chosen to match the experimental concentrations in swollen Nafion, i.e. 19.1 DMSO molecules per SO_3^- group or 5.1 ACN molecules per SO_3^- group.[26] Additionally, a configuration of 5.1 DMSO molecules per SO_3^- group was simulated to help differentiate between inherent solvent effects and volume fraction effects. Table I summarizes absorption measurements for ACN, DMSO, and water in lithiated Nafion. The volume fraction of solvent is largest for DMSO, and smallest for ACN. The volume fraction of water is more similar to ACN than DMSO. Conversely, DMSO and water are more similar on the basis of maximal number of solvent molecules per SO_3^- group.

Table I. Absorption of DMSO, ACN, and water by lithiated Nafion according to Reference 26.

Solvent	ACN	DMSO	DMSO[a]	Water
Solvent molecules per SO_3^- group	5.1	19.1	5.1	20
Solvent volume fraction	0.33	0.71	0.40	0.40
Conductivity (mS/cm)	0.0054	1.6	N/A	16.1

[a]Fictitious, to aid interpretation.

Thermalization was performed in an isothermal–isobaric (NPT) ensemble. The external pressure was set to 1 atm throughout the simulations. Temperature was changed during the thermalization process. The initial temperature of the system was $T_0 = 50$ K and the system was heated to $T_1 = 500$ K over 1 ns, where the system was equilibrated for 10 ns. Afterwards, the system was cooled to $T_2 = 300$ K over 10 ns. This thermalization process allows the initial low-density structure to anneal into a system with realistic density. The density of the DMSO system increased from 0.0051 g/cm^3 to 1.36 g/cm^3. The initial density of the system with ACN was 0.0026 g/cm^3 and the final density was 1.59 g/cm^3. Finally, an 8−10 ns NPT simulation at 300 K was used to calculate mobility.

Results and Discussion

Structure of lithiated nafion imbibed with DMSO and ACN.— Snapshots of the DMSO systems after thermalization are shown in Figure 3. For better visualization, a snapshot of the system with $\lambda = 19.1$ with all DMSO molecules removed is shown in Figure 3a, and the DMSO molecules are shown separately in Figure 3b. Microphase separation is evident in these snapshots. One phase is nonpolar and formed by PFSA backbone molecules. The second phase is

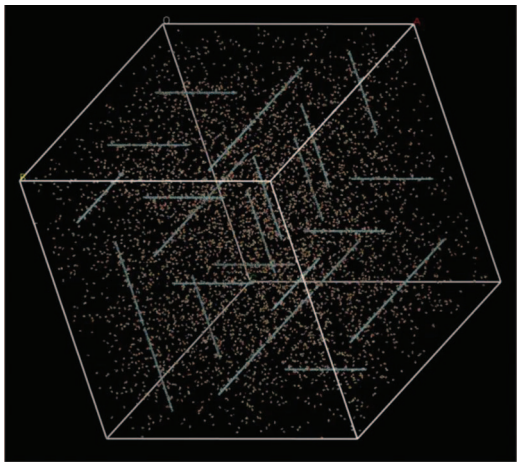

Figure 2. Initial structure before thermalization: blue lines are PFSA chains randomly oriented along the x, y, or z coordinate axes; small points are chaotically orientated solvent molecules.

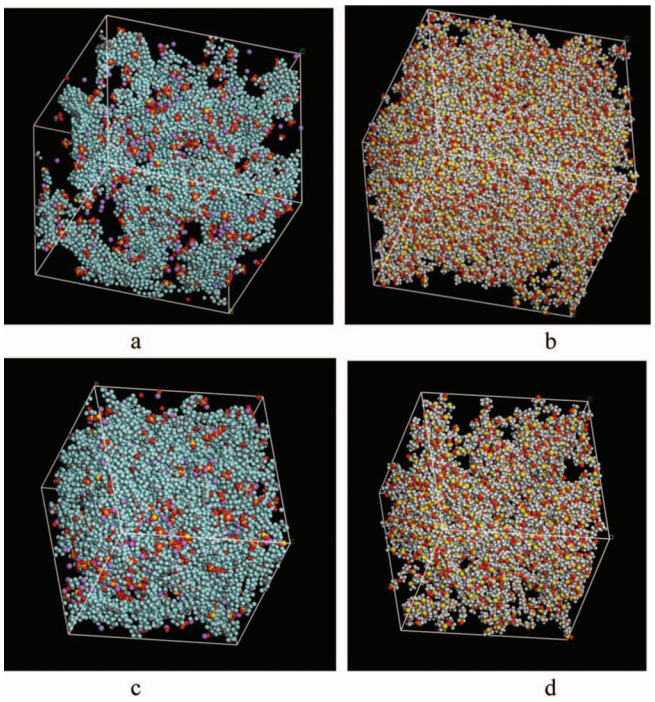

Figure 3. Snapshots of Nafion + DMSO systems after thermalization: (a) with DMSO removed at $\lambda = 19.1$, (b) the removed DMSO at $\lambda = 19.1$, (c) with DMSO removed at $\lambda = 5.1$, (d) the removed DMSO $\lambda = 5.1$.

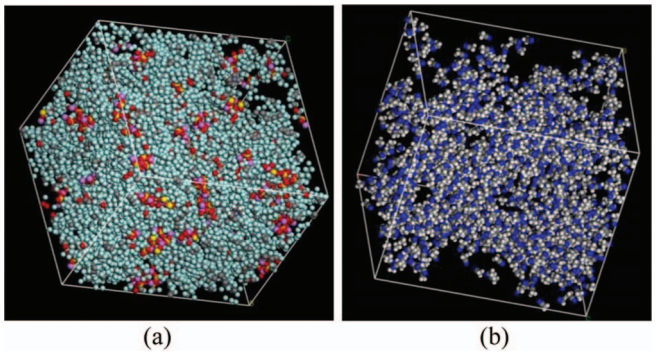

Figure 4. Snapshots of the Nafion + ACN system after thermalization: (a) with ACN removed, (b) the removed ACN.

polar and formed by solvent molecules. Sulfur atoms (yellow) in the SO_3^- groups are clearly visible in Figure 3a, indicating that the SO_3^- groups are predominantly located at the interface between the phases. One can see that a fraction of the Li^+ ions (violet) is coupled with SO_3^- groups and the rest are free Li^+ ions located in the DMSO phase (hollow space in Figure 3a). The simulations with less DMSO, $\lambda = 5.1$, are shown in Figures 3c and 3d. Microphase separation remains evident, although to a smaller degree.

Snapshots of the thermalized ACN system are shown in Figure 4. The system with ACN removed is shown in Figure 4a, while ACN molecules are displayed separately in Figure 4b. Micro-phase separation is observed in this case as well. One phase is non-polar and formed by PFSA backbone molecules (see Figure 4a). The second phase is polar and formed by solvent molecules (see Figure 4b). One can see that Li^+ ions, violet in color, are mostly coupled with SO_3^- groups (sulfur atoms are yellow in Figure 4a).

To make the coupling of Li^+ ions and SO_3^- groups more evident, only SO_3^- groups and Li^+ ions in Nafion + DMSO are shown in Figure 5a ($\lambda = 19.1$) and in Nafion + ACN in Figure 5b. SO_3^- groups and Li^+ ions are distributed almost uniformly throughout the simulation volume in Nafion + DMSO and only a fraction of the Li^+ ions is tightly coupled to SO_3^- groups. On the contrary, in Nafion + ACN, SO_3^- groups and Li^+ ions aggregate in clusters that consist of several SO_3^- groups and Li^+ ions. Free Li^+ ions are not observed in Nafion + ACN.

To calculate the fractions of Li^+ ions that are free and coupled with SO_3^- groups, the probability density distribution of the distance between a Li^+ ion and the nearest SO_3^- group was calculated through simulated MD trajectories for Nafion + DMSO and Nafion + ACN. The distance between Li^+ ions and SO_3^- groups was determined as the distance between Li^+ and the nearest oxygen atom of the SO_3^- group. In Nafion + ACN, one sharp peak near 1.75 Å is observed in Figure 6. This demonstrates that all Li^+ ions are strongly coupled with SO_3^- groups in our MD simulation, and the mean distance between coupled Li^+ and SO_3^- is about 1.75 Å. A sharp peak near 1.75 Å is also observed in Nafion + DMSO. In addition, the distribution for Nafion

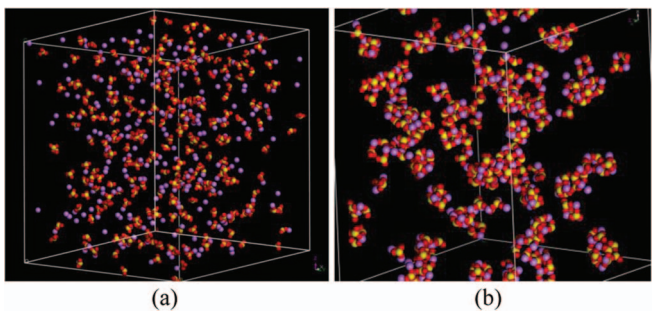

Figure 5. SO_3^- groups and Li^+ ions in thermalized systems: (a) DMSO at $\lambda = 19.1$, (b) ACN at $\lambda = 5.1$.

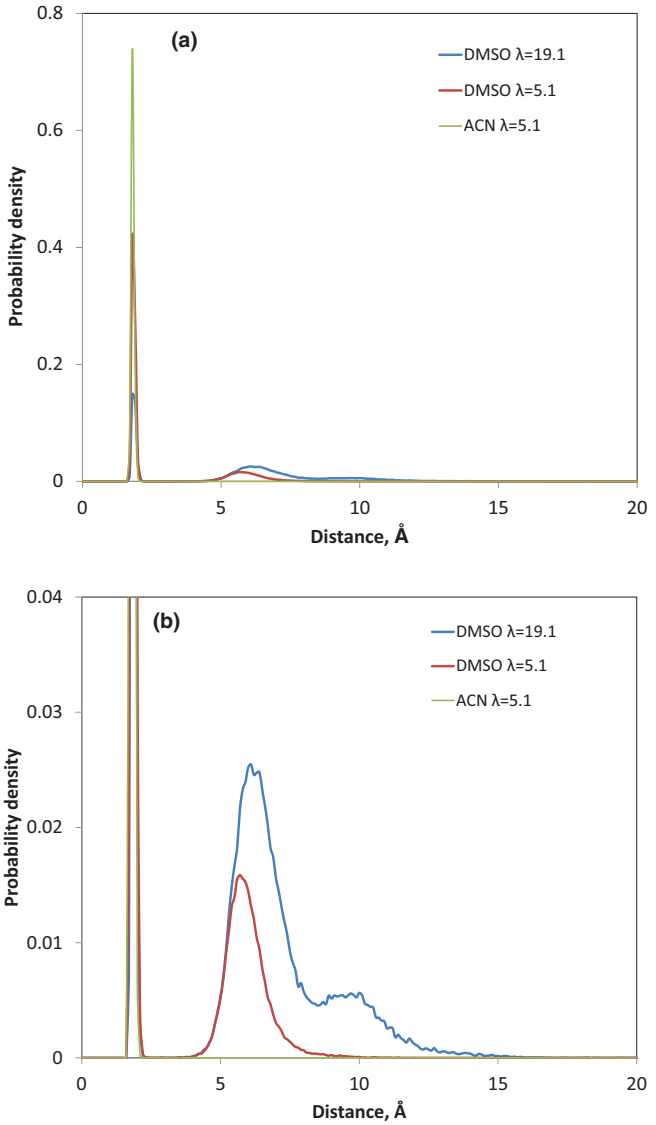

Figure 6. Probability density distribution of the distance from a Li^+ ion to the nearest oxygen on a SO_3^- group. Plots (a) and (b) are the same except for the axes scales.

+ DMSO has a broad peak near 6.5 Å both for $\lambda = 19.1$ and $\lambda = 5.1$, where λ represents the number of solvent molecules per SO_3^- group. This broad peak in Figure 6 corresponds to free Li^+ ions. Thus, only a fraction of the Li^+ is strongly coupled with SO_3^- groups in Nafion + DMSO. The remaining Li^+ ions are uncoupled and distributed in the bulk of the polar phase. In addition, the single strong peak observed at 1.75 Å for ACN reveals the poor solvation and distribution of ACN throughout the system. This structural distribution difference between DMSO and ACN provides initial insight into the diffusivity and conductivity differences observed between the two solvents.

The fractions of coupled and free Li^+ ions are calculated through integrals of the probability density distribution over the narrow and broad peaks. The calculated fractions of free Li^+ ions in Nafion with DMSO are about 64% for $\lambda = 19.1$ and 24% for $\lambda = 5.1$. The results for DMSO with $\lambda = 5.1$ indicate that the lack of free Li^+ in ACN is not dictated solely by low solvent concentration; instead it is a result of differences between the two solvents. Radial distribution functions (RDFs) are presented in the appendix and supplementary material that reveal the structures of the solvation shells of Li^+ in DMSO and ACN.

To calculate the average size of a polar phase (solvent) cluster, the probability density distribution of the distance between a solvent

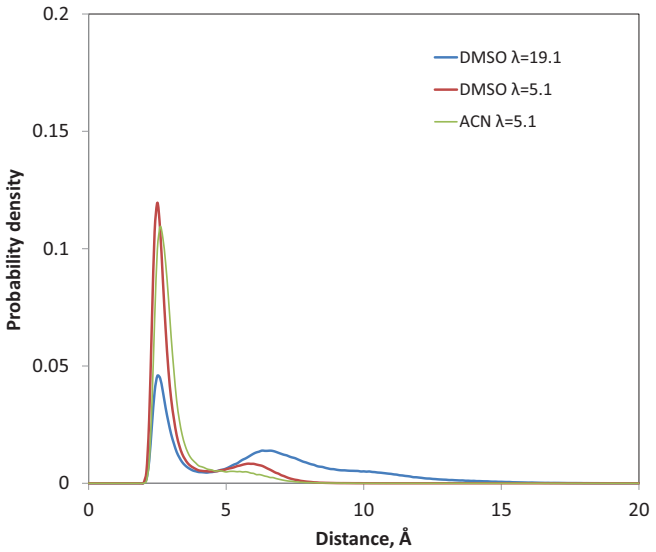

Figure 7. The probability density distribution of the distance between solvent molecules and the nearest backbone atom.

molecule and the nearest backbone atom was calculated and is shown in Figure 7. In Nafion + ACN, one narrow peak is observed near 3.2 Å which is close to the van der Waals radius. All solvent molecules are in contact with the PFSA backbone and an ACN cluster consists of several molecules. In the case of Nafion + DMSO with $\lambda = 19.1$, the distribution is much broader and the average distance is estimated to be 7 Å. This distance can be interpreted as the average radius of a solvent cluster. For DMSO at $\lambda = 5.1$, the distribution also has the second peak, though not as pronounced as the peak for $\lambda = 19.1$. However, in all cases the polar phase is a connected cluster penetrating the entire simulation box as seen in Figures 3b, 3d, and 4b.

Diffusion simulations.—The mobility of different components of the system was estimated during a portion of the MD run lasting 8–10 ns. The mean square displacement of different components (PFSA chains, Li^+ ions, SO_3^- groups, or solvent molecules) was calculated as

$$\left\langle \Delta^2(t) \right\rangle = \frac{1}{N} \sum_{i=1}^{N} |\vec{r}_i(t) - \vec{r}_i(0)|^2, \qquad [1]$$

where $\vec{r}_i(t)$ is the position of the *i-th* particle at time t, $\vec{r}_i(0)$ is the position of the *i-th* particle at $t = 0$, and N is the number of particles. Mean square displacements for PFSA chains, Li^+ ions, SO_3^- groups, and solvent molecules were calculated with equation 1 and are presented in Figure 8. The mean square displacement of PFSA chains is an average of the polymer atoms, not the center of mass. The nearly complete overlap of displacement curves for Li^+ ions and SO_3^- groups for Nafion + ACN is the result of total coupling of Li^+ ions with SO_3^- groups.

Computational limitations restrict us to simulations that last tens of nanoseconds. At short times, the simulated transport regime can be transient to the true diffusive regime where mean square displacement (MSD) is proportional to time. The transient regime is caused by the presence of two length scales in the Nafion-solvent system with phase separation. The smaller scale is equal to the mean size of a cluster in the polar phase. The larger scale is the size of the sample which is much larger than a cluster. At small time and length scales, a diffusing solvent molecule or Li^+ ion does not interact with the cluster walls and moves as in pure solvent. At large time and length scales the solvent molecules and Li^+ ions diffuse through a tortuous and branched polar phase as in an effective continuum medium with renormalized diffusion coefficient and MSD is proportional to time. At intermediate time and length scales a transition from diffusion in pure solvent to diffusion in effective continuum medium is realized. In this regime MSD can be proportional to t^γ, where $\gamma \neq 1$. The dynamics of the polymer system complicate the situation even more.[45–47] A double logarithmic plot of MSD versus time for ACN molecules and Li^+ ions in Nafion + ACN is shown in Figure 2 of the supplementary material. The slope of the plots is close to 0.8 which means that in our simulations with ACN the MSD is proportional to $t^{0.8}$. Thus, we do not see true diffusion in these simulations. However, for our purposes we treated MD trajectories in terms of diffusive transport and calculate apparent diffusion coefficients. While this approach is not mathematically rigorous, it is sufficient to characterize the large differences in mobility between the ACN and DMSO systems at reasonable computational cost.

Diffusion coefficients were calculated from the linear regression of the mean square displacement $\langle \Delta^2(t) \rangle$

$$D = \frac{1}{6t} \left\langle \Delta^2(t) \right\rangle \qquad [2]$$

The diffusion coefficients obtained are summarized in Table II. The final row contains ratios of diffusion coefficients in Nafion + DMSO divided by diffusion coefficients in Nafion + ACN. The diffusion coefficients of PFSA atoms and SO_3^- groups in Nafion + DMSO are about an order of magnitude higher than in Nafion + ACN. This is partially attributable to the higher solvent volume fraction in Nafion + DMSO than in Nafion + ACN. The higher volume fraction of solvent enhances the mobility of the polymer matrix.

The calculated diffusion coefficients of solvent molecules (DMSO or ACN) are very similar in Nafion + DMSO and Nafion + ACN as shown in Table III. On the other hand, the calculated diffusion coefficient of DMSO molecules in neat solvent is 2.3× larger than in Nafion (see Table III), while the calculated diffusion coefficient of ACN in neat solvent is 9.6x larger than in Nafion. The substantially greater reduction of solvent diffusion in the case of ACN is a consequence of the relatively small volume fraction of solvent in Nafion + ACN. The final column in Table III shows the tortuosity calculated for the two solvents from the equation $D_{Nafion} = D_{bulk}\varepsilon\tau^{-1}$. Both tortuosities are reasonable, suggesting that the increase in tortuosity could be substantially responsible for the reduction in diffusivity. For the sake of comparison, the calculated diffusion coefficient of water in Nafion ($\varepsilon = 0.40$) is 3.4×10^{-6},[23] which is similar to the values for DMSO and ACN.

Table IV summarizes the diffusion coefficients of Li^+ in pure DMSO and ACN and in Nafion imbibed with the same solvents. In the case of ACN, the diffusion coefficient of Li^+ drops dramatically from the pure solvent to Nafion. This drop is much more dramatic than the decline in the diffusivity of ACN molecules (see Table IV) which demonstrates that the coupling of Li^+ with SO_3^- groups is responsible and that the increase in tortuosity is of secondary importance. The extreme tortuosity calculated for Li^+ in ACN + Nafion clearly emphasizes the role of coupling. The calculated diffusion coefficient of Li^+ coincides with the diffusion coefficient of SO_3^- groups in Nafion + ACN. This is a consequence of complete coupling of Li^+ ions and SO_3^- groups. In Nafion + ACN, a Li^+ ion can only move together with an associated SO_3^- group. The diffusivity of Li^+ ions in Nafion + DMSO is higher than the diffusivity of SO_3^- groups because free Li^+ ions diffuse independently and have higher mobility than coupled Li^+ ions. Only free Li^+ ions determine the macroscopic conductivity of the ionomer.

Calculation of ionic conductivity.—The mobility of free Li^+ ions determines the conductivity of the membrane. The equation for the mean square displacement of Li^+ ions can be written as

$$\left\langle \Delta^2(t) \right\rangle_{Li} = \frac{N_c}{N} \frac{\sum_{i=1}^{N_c} \left| \vec{r}_i^{\,c}(t) - \vec{r}_i^{\,c}(0) \right|^2}{N_c} + \frac{(N - N_c)}{N} \frac{\sum_{i=1}^{N-N_c} \left| \vec{r}_i^{\,f}(t) - \vec{r}_i^{\,f}(0) \right|^2}{(N - N_c)} \qquad [3]$$

Here N is the total number of Li^+ ions, N_c is the number of Li^+ ions tightly coupled with SO_3^- groups, *(N-N$_c$)* is the number of free Li^+

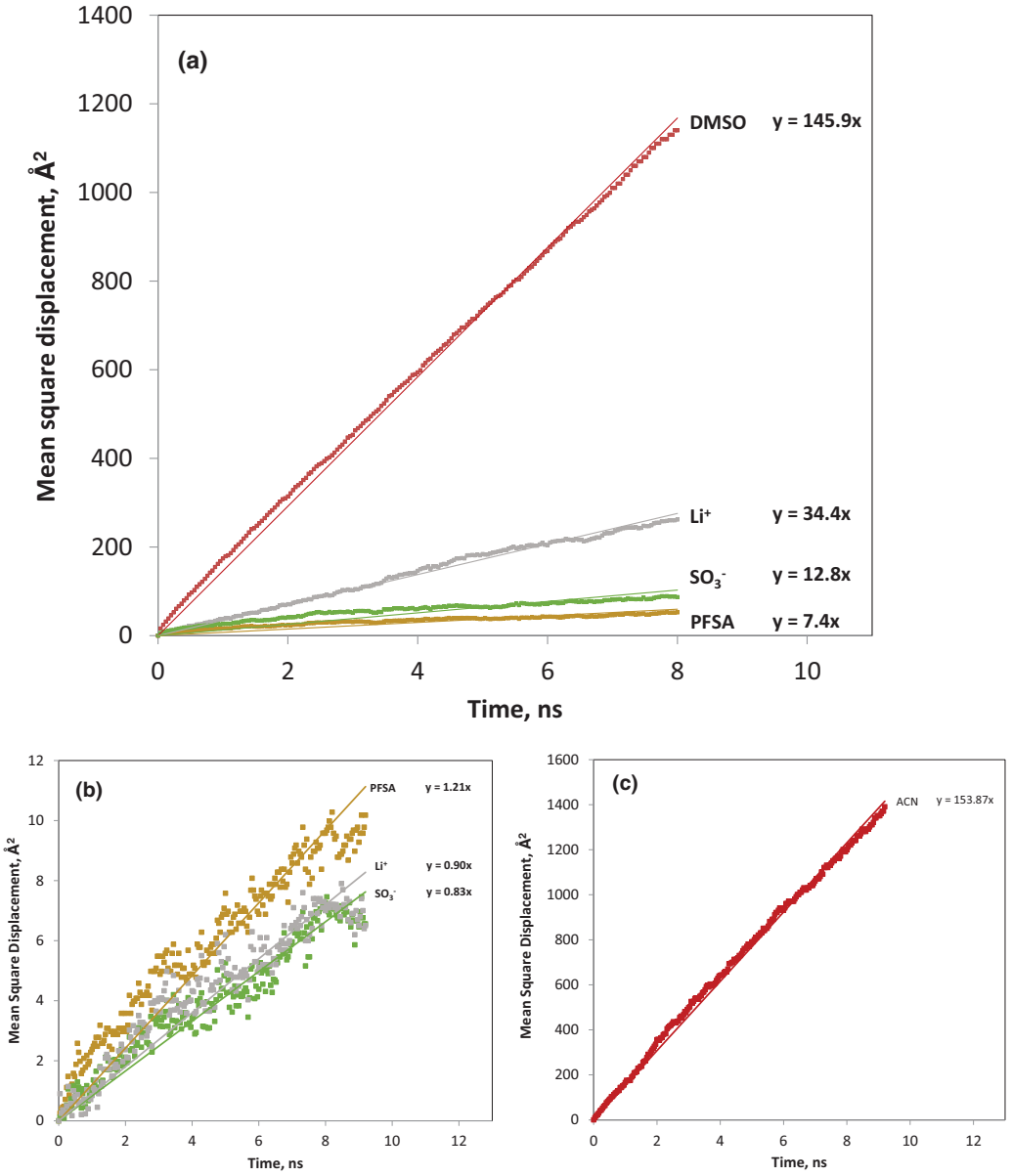

Figure 8. Mean square displacements of PFSA chains, lithium ions, SO_3^- groups, and solvent molecules: (a) DMSO at $\lambda = 19.1$, (b) and (c) ACN.

ions, $\vec{r}_i^{\,c}$ is the position of the *i-th* coupled ion and $\vec{r}_i^{\,f}$ is the position of the *i-th* free ion. Equation 3 can be simplified to

$$\left\langle \Delta^2(t) \right\rangle_{Li} = f \left\langle \Delta^2(t) \right\rangle_{Li}^{c} + (1-f) \left\langle \Delta^2(t) \right\rangle_{Li}^{f} \qquad [4]$$

Here f is the fraction of coupled Li^+ ions, $\langle \Delta^2(t) \rangle_{Li}^{c}$ is mean square displacement of coupled Li^+ ions, and $\langle \Delta^2(t) \rangle_{Li}^{f}$ is mean square displacement of free Li^+ ions. Substituting Equations 4 into 2 we obtain

$$D_{Li} = f D_{Li}^{c} + (1-f) D_{Li}^{f} \qquad [5]$$

Here D_{Li} is the diffusion coefficient of all Li^+ ions (free and coupled with SO_3^- groups), $D_{Li}{}^f$ is the diffusion coefficient of free Li^+ ions and $D_{Li}{}^c$ is diffusion coefficient of coupled Li^+ ions. Taking advantage of the fact that the diffusion coefficient of coupled Li^+ ions is equal to the diffusion coefficient of SO_3^- groups, D_{SO3}, we obtain the following

Table II. Calculated diffusion coefficients in Nafion + DMSO and Nafion + ACN, cm²/s.

	PFSA	Li^+	SO_3^-	Solvent
DMSO, $\lambda = 19$	$(2.3 \pm 1.3) \times 10^{-7}$	$(6.0 \pm 0.6) \times 10^{-7}$	$(3.9 \pm 2.1) \times 10^{-7}$	$(2.7 \pm 0.2) \times 10^{-6}$
ACN	$(3.1 \pm 1.1) \times 10^{-8}$	$(1.9 \pm 0.6) \times 10^{-8}$	$(1.9 \pm 0.6) \times 10^{-8}$	$(2.8 \pm 0.2) \times 10^{-6}$
Ratio	7.4	31.6	20.5	0.96

Table III. Solvent diffusion coefficients in Nafion and neat.

Solvent	D_{bulk} ($\times 10^6$, cm^2/s)	D_{Nafion} ($\times 10^6$, cm^2/s)	Ratio	Tortuosity
DMSO	6.33	2.74	2.3	1.6
ACN	27[30]	2.80	9.6	3.2
Ratio	0.23	0.98		

Table IV. Li^+ diffusion coefficients.

Solvent	D_{bulk} ($\times 10^6$, cm^2/s)	D_{Nafion} ($\times 10^6$, cm^2/s)	Ratio	Tortuosity
DMSO	2	0.6	3.3	2.3
ACN	15	0.02	750	248
Ratio	0.13	30		

equation for the diffusion coefficient of free Li^+ ions

$$D_{Li}^{f} = \frac{D_{Li} - fD_{SO3}}{1 - f} \quad [6]$$

The mobility of free Li^+ is calculated from the Nernst-Einstein relation

$$u_{Li} = \frac{q D_{Li}^{f}}{kT}, \quad [7]$$

where $q = 1.6 \times 10^{-19}$ C is the elementary charge, k is the Boltzmann constant, and T = 300 K is the absolute temperature. The ionic conductivity of Li^+ is calculated according to

$$\sigma_{Li} = Fc^{f}u_{Li}, \quad [8]$$

where $c^f = (1 - f)c$ is the concentration of free Li^+ ions, and c is the total concentration of Li^+ ions.

Taking into account Equations 6–8 we obtain the final equation for Li^+ conductivity

$$\sigma_{Li} = \frac{Fcq\,(D_{Li} - fD_{SO3})}{kT} \quad [9]$$

Our calculations give $\sigma_{Li} \approx 0.9$ mS/cm (see Table V) for Nafion + DMSO which agrees satisfactorily with the experimental values of 1.09 ± 0.09 μS/cm measured in this work and 1.6 mS/cm reported by Doyle et al.[26] The ionic conductivity of lithiated Nafion + ACN is very small because the fraction of free Li^+ ions is essentially zero in our simulation. This statement qualitatively agrees with the Nafion + ACN ion conductivities of 1.43 ± 0.35 μS/cm and 5.36 μS/cm[26] measured in this work and reported by Doyle et al., respectively. These conductivities are two orders of magnitude lower than Nafion + DMSO.

Conclusions

A molecular dynamic model of lithiated Nafion swelled in the nonaqueous solvents DMSO and ACN was developed. The model was validated by calculating the self-diffusion coefficient of DMSO in pure DMSO. The model prediction for the self-diffusion coefficient of DMSO, 6.3×10^{-6} cm^2/s, agrees with simulation results reported in the literature,[30] 5×10^{-6} cm^2/s. The model predicts that the degree of dissociation of Li^+ ions and SO_3^- groups in Nafion + DMSO is about 64%, while the degree of dissociation in Nafion + ACN is approximately zero. These results explain the two orders of magnitude difference in the conductivities of Nafion + DMSO and Nafion + ACN observed experimentally. The calculated ionic conductivity of Nafion + DMSO is $\sigma_{Li} \approx 0.9$ mS/cm, which agrees satisfactorily with the experimental value $\sigma_{Li} \approx 1.09$ mS/cm. The apparent diffusion coefficient of the PFSA matrix at small time scales in Nafion + DMSO is approximately one order of magnitude higher than in Nafion + ACN. The polymer matrix is more mobile in DMSO than in ACN because more solvent is present.

Experimental values of solvent uptake were used in the simulations with 19.1 DMSO molecules per SO_3^- group and 5.1 ACN molecules per SO_3^- group. In order to elucidate the impact of solvent concentration on Li^+ and SO_3^- dissociation, simulations were also completed with 5.1 DMSO molecules per SO_3^- group. Fewer free Li^+ ions were found for the case with $\lambda = 5.1$ compared to $\lambda = 19.1$; however, our results demonstrate that the ability to dissociate ionic pairs impacts the free ionic concentrations in Nafion more than the amount of swelling.

We conclude from the simulations that the ionic conductivity of Nafion is mostly governed by the concentration of free Li^+ ions, i.e. by the degree of dissociation of Li^+ and SO_3^- pairs, not by the ionic mobility in the pure solvents. We speculate that the degree of dissociation of the lithium salt of Nafion in different solvents correlates with the degree of dissociation of lithium triflate ($LiCF_3SO_3$) in the same solvents. Therefore, the experimental or modeled degree of dissociation of lithium triflate in different solvents can be used for faster selection of nonaqueous solvents for Nafion.

Acknowledgments

Work at UTRC was supported as part of the Joint Center for Energy Storage Research, an Energy Innovation Hub funded by the U.S. Department of Energy, Office of Science, Basic Energy Sciences. The authors acknowledge the Joint Supercomputer Center of the Russian Academy of Science for computation resources granted.

Appendix: The Structures of Li^+ Ion Solvation Shells

Radial distribution functions (RDFs) were analyzed in order to understand the structures of the solvation shells of Li^+ ions in DMSO and ACN. The RDF between atoms of types i and j is calculated as[48]

$$RDF(r) = \frac{1}{\rho 4\pi r^2 \delta r} \frac{\sum_{t=1}^{T}\sum_{j=1}^{N} \Delta N(r \to r + \delta r)}{NT}, \quad [A1]$$

where T is the total number of snapshots of the MD trajectory used, ΔN is the number of particles of type j around a particle of type i within a thin spherical layer from r to r+δr, N is the total number of particles of type i and ρ is the average density of particles of type j. The number of particles of type j around a particle of type i within a spherical layer from r to r+Δr is calculated from the RDF(r) as follows

$$N_{ij}(r, r + \Delta r) = 4\pi\rho \int_{R}^{R+\Delta R} RDF(r) r^2 dr \quad [A2]$$

The RDFs for DMSO with $\lambda = 19.1$ are presented in Figure 3 of the supplementary material. The RDF Li-S(of SO_3^-) shows a distinct peak at 3.2 Å. Integration over this peak according to (A2) gives 0.34 for the number of SO_3^- groups coupled with one Li^+ ion, $N_{Li,S(SO3)}(2.5, 3.5) = 0.34$. This value is in good agreement with 32% of Li^+ ions coupled obtained from the probability density distribution of the distance between a Li^+ ion and the nearest SO_3^- group. This means that the majority of Li^+- SO_3^- aggregates consists of one Li^+ ion and one SO_3^- group. The RDF for Li-O(of SO_3-) has two distinct peaks. The first peak is at 1.8 Å. Integration over this peak gives the same value of 0.34: $N_{Li,O(SO3)}(1.5, 2.5) = 0.34$. This peak corresponds to coupling of a Li^+ ion with one of the three oxygen atoms on a SO_3^- group. The second peak at 4.2 Å corresponds to the distances to the other two oxygen atoms on a SO_3^- group. Integration over this peak gives 0.68 which is exactly twice the integral over the first peak:

Table V. Fraction of free Li^+ (1-f), Li^+ concentration, diffusion coefficient D_{Li}^{free}, mobility u_{Li}, and ionic conductivity σ_{Li}.

	(1-f)	c [mol/l]	D_{Li}^{free} [cm^2/s]	u_{Li} [C · s/kg]	$\sigma_{Li,MD}$ [μS/cm]	$\sigma_{Li,exp}$ [μS/cm]
DMSO, $\lambda = 19.1$	0.64	0.52	7.2×10^{-7}	2.8×10^{-9}	900	1090
DMSO, $\lambda = 5.1$	0.24	1.12	1.7×10^{-8}	6.4×10^{-11}	20	N/A
ACN	0	1.21	-	-	0	1.43

$N_{Li,O(SO3)}(2.5, 4.7) = 0.68$. This provides additional evidence that one Li^+ ion is usually coupled with one SO_3^- group. The absence of peaks in the RDF for Li-Li indicates that Li^+ ions are not aggregated together.

The RDFs from Li^+ ions to atoms of DMSO are presented in Figure 4 of the supplementary material. These RDFs reflect Li^+ ion solvation which is averaged over free and coupled Li^+ ions. All RDFs show two distinct peaks; a well-pronounced (and sharp for O and S atoms) peak at a short distance and a broad peak at a longer distance which correspond to DMSO molecules in the first and second solvation shells. The positions of the sharp, separated peaks for short distances (1.8 Å for O atoms and 2.5 Å for S atoms) indicate that DMSO molecules are arranged around Li^+ ions to optimize electrostatic interactions. A pyramidal DMSO molecule is orientated next to a Li^+ ion by the vertex with a negatively charged O atom at a distance of 1.8 Å. The integration over the first peak gives 3.5 DMSO molecules in the first solvation shell: $N_{Li,O(DMSO)}(1.5, 2.5) = 3.5$. This average includes free and coupled Li^+ ions. We separately analyzed solvation of free Li^+ ions, Li^+ ions coupled with one SO_3^- group, and, Li^+ ions coupled with two SO_3^- groups. Free Li^+ ions have exactly four DMSO molecules in the first solvation shell. Li^+ ions coupled with one SO_3^- group have exactly three DMSO molecules in the first solvation shell, and Li^+ ions coupled with two SO_3^- groups have exactly two DMSO molecules in the first solvation shell. DMSO molecules are orientated next to Li^+ ions by O atoms, and the distance between Li^+ and an O atom on DMSO is equal to the distance between Li^+ and the nearest O atom on a SO_3^- group (1.8 Å). Thus, Li^+ ions do not distinguish between O atoms on DMSO molecules and on SO_3^- groups. Every Li^+ ion has four O atoms either from DMSO molecules or SO_3^- groups in the first coordination shell.

The solvation shell of Li^+ ions in Nafion + ACN qualitatively differs from that in Nafion + DMSO. The RDF Li-S(of SO_3^-) also shows a distinct peak at 3.2 Å (see Figure 5 of the supplementary material). Integration over this peak gives a value of 2.66 for the number of SO_3^- groups coupled with one Li^+ ion: $N_{Li,S(SO3)}(2.5, 4.0) = 2.66$. This indicates that one Li^+ ion is coupled with several SO_3^- groups. A detailed analysis shows that 1% of Li^+ ions are coupled with one SO_3^- group, 31% of Li^+ ions are coupled with two SO_3^- groups, 60% of Li^+ ions are coupled with three SO_3^- groups, and 8% of Li^+ ions are coupled with four SO_3^- groups. The RDF for Li-Li shows distinct two peaks at 4.7 Å and 5.7 Å. All these facts indicate that aggregates consisting of several Li^+ ions and SO_3^- groups are formed in Nafion + ACN. The RDF Li-O(of SO_3^-) has two distinct peaks as in Nafion + DMSO. The first peak at 1.8 Å corresponds to the coupling between a Li^+ ion and one of O atoms on a SO_3^- group. Integration over this peak gives 2.6: $N_{Li,O(SO3)}(1.5, 2.5) = 2.6$.

The RDFs from Li^+ ions to the atoms on ACN molecules are presented in Figure 6 of the supplementary material. All RDFs show one distinct peak. These peaks are located at 2.0 Å, 3.1 Å, 4.5 Å, 5.0 Å for Li-N, Li-C1, Li-C2, Li-H RDFs, correspondingly. The distance between peaks for Li-N and Li-C1 is about 1.6 Å which is close to the N-C1 bond length (1.5 Å). The distance between peaks for Li-C1 and Li-C2 is approximately equal to the C1-C2 bond length (1.4 Å). Because ACN molecules are linear, they are radially orientated with respect to Li^+ ions. Integration over the first peak of the Li-N RDF gives 1.4 ACN molecules in the first solvation shell of Li^+ ions: $N_{Li,N(ACN)}(1.5, 3.0) = 1.4$. The Li-N RDF has second peak at 6.4 Å, which corresponds to the second solvation shell. We separately analyzed solvation of Li^+ ions coupled with different numbers of SO_3^- groups. It was found that for Li^+ ions coupled with 1, 2, 3, and 4 SO_3^- groups the average number of ACN molecules in the first solvation shell is 3.2, 2.1, 1.1, and 0.1, correspondingly. Thus, the total average number of SO_3^- groups and ACN molecules in the first coordination shell of Li^+ ion is about 4.1.

References

1. R. Yadav and P. S. Fedkiw, *J. Electrochem. Soc.*, **159**, B340 (2012).
2. D. R. Morris and X. Sun, *J. Appl. Polym. Sci.*, **50**, 1445 (1993).
3. Y. Sone, P. Ekdunge, and D. Simonsson, *J. Electrochem. Soc.*, **143**, 1254 (1996).
4. M. N. Tsampas, A. Pikos, S. Brosda, A. Katsaounis, and C. G. Vayenas, *Electrochim. Acta*, **51**, 2743 (2006.)
5. T. A. Zawodzinski, C. Derouin, S. Radzinski, R. J. Sherman, V. T. Smith, T. E. Springer, and S. Gottesfeld, *J. Electrochem. Soc.*, **140**, 1041 (1993).
6. A. C. Barbati and B. J. Kirby, *Langmuir*, **30**, 1985 (2014).
7. T. Soboleva, Z. Xie, Z. Shi, E. Tsang, T. Navessin, and S. Holdcroft, *J. Electroanal. Chem.*, **622**, 145 (2008).
8. J. Lee, C. W. Yi, and K. Kim, *B. Kor. Chem. Soc.*, **33**, 1788 (2012).
9. S. Slade, S. A. Campbell, T. R. Ralph, and F. C. Walsh, *J. Electrochem. Soc.*, **149**, A1556 (2002).
10. S. Cui, J. Liu, M. E. Selvan, D. J. Keffer, B. J. Edwards, and W. V. Steele, *J. Phys. Chem. B*, **111**, 2208 (2007).
11. X. Zhou, Z. Chen, F. Delgado, D. Brenner, and R. Srivasta, *J. Electrochem. Soc.*, **154**, B82 (2007).
12. A. Vishnyakov and A. V. Neimark, *J. Phys. Chem. B*, **105**, 9586 (2001).
13. S. S. Jang, V. Molinero, T. Cagin, and W. A. Goddard III, *J. Phys. Chem. B*, **108**, 3149 (2004).
14. E. Allahyarov and P. L. Taylor, *J. Phys. Chem. B*, **113**, 610 (2009).
15. T. Ohkubo, K. Kidena, N. Takimoto, and A. Ohira, *J. Mol. Model.*, **17**, 739 (2011).
16. T. Ohkubo, K. Kidena, N. Takimoto, and A. Ohira, *J. Mol. Model.*, **18**, 5330 (2012).
17. G. S. Hwang, M. Kaviany, J. T. Gostick, B. Kientiz, A. Z. Weber, and M. H. Kim, *Polymer*, **52**, 2584 (2011).
18. D. W. M. Hofmann, L. Kuleshova, and B. D'Aguanno, *J. Mol. Model.*, **14**, 225 (2008).
19. H. Sun, M. Yu, Z. Li, and S. Almheiri, *Journal of Chemistry*, ID 169680 (2015).
20. Y.-L. S. Tse, A. M. Herring, K. Kim, and G. A. Voth, *J. Phys. Chem. C*, **117**, 8079 (2013).
21. K. Morohoshi and T. Hayashi, *Polymers*, **5**, 56 (2013).
22. H. Abroshan, H. Akbarzadeh, F. Taherkhani, and G. Parsafar, *Mol. Phys.*, **109**, 709 (2011).
23. A. Chertovich, P. G. Khalatur, and A. R. Khokhlov, *Compos. Interface*, **16**, 547 (2009).
24. Q. Zhao, N. Carro, H. Y. Ryu, and J. Benzinger, *Polymer*, **53**, 1267 (2012).
25. V. M. Barragan, C. Ruiz-Bauza, J. P. G. Villaluenga, and B. Seoane, *J. Power Sources*, **130**, 22 (2004).
26. M. Doyle, M. E. Lewittes, and S. A. Roelofs, *J. Membr. Sci.*, **184**, 257 (2001).
27. I. L. Escalante-Garcia, J. S. Wainright, L. T. Thompson, and R. F. Savinell, *J. Electrochem. Soc.*, **162**, A363 (2015).
28. N. Mozhzukhina, M. P. Longinotti, H. R. Corti, and E. J. Calvo, *Electrochim. Acta*, **154**, 456 (2015).
29. C. O. Laoire, S. Mukerjee, and K. M. Abraham, *J. Phys. Chem. C*, **114**, 9178 (2010).
30. R. Semino, G. Zaldivar, E. J. Calvo, and D. Laria, *J. Chem. Phys.*, **141**, 214509 (2014).
31. M. Doyle, M.E. Lewittes, M.G. Roelofs, and S.A. Perusich, *J. Phys. Chem. B*, **105**, 9387 (2001).
32. R.J. Klein and J. Runt, *Phys. Chem. B*, **111**, 13188 (2007).
33. S. Sachan, C.A. Ray, and S.A. Perusich, *Polym. Eng. Sci.*, **42**, 1469 (2002).
34. E. Soolo, D. Brandell, A. Liivat, H. Kasemägi, T. Tamm, and A. Aabloo, *Electrochimica Acta*, **55**, 2587 (2010).
35. Z. Samec, A. Trojanek, and J. Langmaier, *J. Electrochem. Soc.*, **144**, 4236 (1997).
36. I.A. Stenina, Ph. Sistat, A.I. Rebrov, G. Pourcelly, and A.B. Yaroslavtsev, *Desalination*, **170**, 49 (2004).
37. G. Suresh, Y.M. Scindia, A.K. Pandey, and A. Goswami, *J. Membr. Sci.*, **250**, 39 (2005).
38. G. Herlem, B. Fahys, M. Herlem, and J.-F. Penneau, *J. Solution Chem.*, **28**, 223 (1999).
39. X. Li, F. Li, Y. Shi, Q. Chen, and H. Sun, *Phys. Chem. Chem. Phys.*, **12**, 14543 (2010).
40. M. L. Strader and S. E. Feller, *J. Phys. Chem. A*, **106**, 1074 (2002).
41. A. M. Nitkin and A. P. Lyubartsev, *J. Comput. Chem.*, **28**, 2020 (2007).
42. X. L. Dang, *J. Chem. Phys.*, **96**, 6970 (1992).
43. S. Plimpton, *J. Comput. Phys.*, **117**, 1 (1995).
44. *Hockney and Eastwood, Computer Simulation Using Particles*, Adam Hilger, New York, pp. 287–325 (1989).
45. M. Doi and S. F. Edwards, *The Theory of Polymer Dynamics*, Clarendon Press, Oxford, p. 140 (1986).
46. P. G. de Gennes, *Physics*, **3**, 37 (1967).
47. S. F. Burlatskii, *Doklady Akademii Nauk SSSR*, **288**, 155 (1986).
48. H. Sun, M. Yu, Zh. Li, and S. Almheiri, *Journal of Chemistry*, ID 169680 (2015).